



The 9th International Conference “ENVIRONMENTAL ENGINEERING”

22–23 May 2014, Vilnius, Lithuania

SELECTED PAPERS

eISSN 2029-7092 / eISBN 978-609-457-640-9

Available online at <http://enviro.vgtu.lt>

Section: Technologies of Geodesy and Cadastre

Image data fusion for flood plain mapping

Michał Kedzierski, Michałina Wilinska, Damian Wierzbicki, Anna Fryskowska, Paulina Delis

*Department of Remote Sensing and Photogrammetry, Institute of Geodesy, Faculty of Civil Engineering and Geodesy,
Military University of Technology, 2 gen. S. Kaliskiego st., 00-908 Warsaw, Poland*

Abstract

Mini multispectral sensors are an insufficient source of imagery to perform appropriate analyses, due to the low spatial resolution of imagery. Therefore, in many cases it is necessary to conduct data fusion. However, using common pansharpener methods may not be sufficient. Therefore, the authors propose a new method for processing and sharpening multispectral data acquired with a mini multispectral camera, for mapping purposes, especially in flooded areas and flood plains, in rapid time. The proposed algorithm of sharpening is based on the use of the decorrelation process of multispectral images and their transformation to the YCBCR color space, where the luminance component is converted to the blue band of the high resolution image and then an inverse transformation to the RGB color space is performed, resulting in imagery with a high spatial and spectral resolution. The results of our research were compared with pansharpened multispectral images generated using classical methods: IHS, PCA, Brovey, Ehlers, wavelet and multiplicative transforms. Moreover, an assessment of a quality of the sharpened spectral images by determining: R-RMSE, ERGAS and Q Index indicators was performed.

Keywords: mapping technology; data fusion; pansharpener; multispectral images; flood plain.

1. Introduction

High spatial and spectral resolutions are necessary to perform various complex analyses concerning image interpretation and other remote sensing tasks [8]. Fused data are most commonly used for image classification (eg distinguishing between different types of fields) [25], for the monitoring of urban and industrial agglomerations [28] and rarely for mapping areas at risk of flooding [3]. The fusion of fine spatial information from a high spatial resolution panchromatic (PAN) image with low spatial resolution multispectral (MS) images to get high spatial resolution MS images is known as pan-sharpening [7], [6], [21], [23], [24]. Pansharpener has been an active area of research for more than a decade, and many pansharpener methods and their modifications have been proposed. In particular, the following methods should be distinguished: the Intensity–Hue–Saturation (IHS) method [8], Brovey Transform (BT) [27], Principal Component Analysis (PCA) [6], Multiplicative Transform (MT) [9], [16] Wavelet Resolution Merge (WRM) [6], [12], [19], and Ehlers Fusion (EF) [7]. Most research focuses on a fusion of panchromatic and multispectral imagery acquired from one or several satellite sensors [15], [17], [18], [32]. However, in recent years, there had been a sudden increase in interest in the acquisition of remote sensing data using UAVs and multispectral optoelectronic sensors mounted on them [14]. It allows for image data acquisition from a low ceiling with much higher temporal and spatial resolutions than that of satellite sensors, both in the visible and near-infrared wavelengths, making the process of monitoring rapid changes of soils, especially on flood plains, possible.

In this paper, the data fusion process (images acquired with a SONY NEX-5N high resolution camera and with a Tetracam MCA 6 multispectral camera) was carried out using standard methods: IHS, PCA, WRM, BT, EF, and MT, which are briefly described. Various combinations of spectral bands and an assessment of the results obtained in terms of interpretation were tested. However, use of classical methods of image data fusion had not produced the expected results. Therefore, in order to improve the results, the authors proposed an original data fusion method dedicated for high resolution imagery data obtained from a non-metric digital camera and multispectral images with a relatively low spatial resolution. In addition, laboratory tests were conducted on the results and they confirmed the possibility of using proprietary methods for image pansharpener for monitoring soils, flooded areas and flood plains.

Corresponding author: Damian Wierzbicki. E-mail address: dwierzbicki@wat.edu.pl

<http://dx.doi.org/10.3846/enviro.2014.216>

© 2014 The Authors. Published by VGTU Press. This is an open-access article distributed under the terms of the [Creative Commons Attribution License](#), which permits unrestricted use, distribution, and reproduction in any medium, provided the original author and source are credited.

2. Proprietary method of pansharpening

As a result of using the above pansharpening methods, images characterized by a high correlation between its spectral bands and with a visible chromatic aberration are generated. Because of that, the authors proposed a method of data fusion. Due to the fact that the MCA camera has six lenses, the created images are shifted in relation to each other. Therefore, it is necessary to conduct their relative orientation in order to form a coherent multispectral image. Usually, the relative orientation of images is performed with an alignment file dedicated to the geometric correction of images from the MCA camera. In the method proposed by the authors, this step is skipped. Much better results, almost devoid of the chromatic aberration effect, were obtained through the independent transformation of each image from the individual spectral bands from the multispectral sensor into the blue band of the SONY NEX-5 image using a 2D polynomial model. At this step, the resampling of six Tetracam MCA images to the spatial resolution of the NEX camera image was performed.

After data pre-processing, a multispectral MCA image decorrelation process was conducted. The decorrelation stretch is a process which is used to enhance the color differences found in a color image. This method includes the removal of the inter-channel correlations found in the input pixels [2]. For the input MCA image X_N , where $N = 6$ (bands), matrices with mean pixel value data for all bands were generated: $A_N = [x_1 \ x_2 \ \dots \ x_n]$, where $x_i = \bar{x}_i - x$ (\bar{x}_i – pixel value for N band, x_i – mean pixel value for N band). Then the covariance matrix $C(N \times N)$ was constructed Eqn (1).

$$C = AA^T \quad (1)$$

The covariance matrix C is symmetric and positive definite. So the eigenvalues of C are real and non-negative. Next we performed eigen-decomposition. The eigenvalues λ_i and the eigenvectors \mathbf{v}_i 's of C satisfy the Eqn (2), where we assume that the eigenvector is normalized, i.e., $\|\mathbf{v}_i\|_2 = 1$

$$C\mathbf{v}_i = \lambda_i\mathbf{v}_i \quad (2)$$

Eqn (2) can be presented in a matrix form Eqn (3), where A is the diagonal matrix with eigenvalues λ_i on its diagonal.

$$CV = VA \quad (3)$$

In the PCA procedure we put λ_i values into A in the following order: $\lambda_1 \geq \lambda_2 \geq \dots \geq \lambda_6$. \mathbf{V} is the matrix consisting of the eigenvectors corresponding to λ_i Eqn (4)'s.

$$V = (\mathbf{v}_1 \ \mathbf{v}_2 \ \dots \ \mathbf{v}_6) \quad (4)$$

So we have the eigen-decomposition of the covariance matrix Eqn (5). The reason that $V^T = V^{-1}$ is due to the fact that C is symmetric and positive definite [26].

$$C = VAV^{-1} \quad (5)$$

Next we constructed PCA image as a linear combination of the eigenvalues matrix \mathbf{V} and input image X_N – Eqn (6)

$$X_{PCA} = \begin{pmatrix} \mathbf{v}_1^T \\ \vdots \\ \mathbf{v}_N^T \end{pmatrix} X_N \quad (6)$$

After that the normalization of the X_{PCA} image presented in the Eqn (7), next inverse PCA transformation Eqn (8) and image stretching Eqn (9) is performed.

$$X_{PCA_norm} = \frac{X_{PCA} - X_{PCA}(\min)}{X_{PCA}(\max) - X_{PCA}(\min)} \quad (7)$$

$$X' = \begin{pmatrix} \mathbf{v}_1^T \\ \vdots \\ \mathbf{v}_N^T \end{pmatrix} X_{PCA_norm} \quad (8)$$

$$X_{decorrelated} = \frac{X' - X'(\min)}{X'(\max) - X'(\min)} \quad (9)$$

The output image can be written in the form: $\mathbf{X}_{decorrelated} = [B_1 \ B_2 \ B_3 \ B_4 \ B_5 \ B_6]^T$, where B is an image band. Two images $I_1 = [B_6 \ B_4 \ B_1]^T$ and $I_2 = [B_5 \ B_3 \ B_2]^T$ were generated and they can be expressed as follows: $I_1 = [R_{641} \ G_{641} \ B_{641}]^T$ and $I_2 = [R_{532} \ G_{532} \ B_{532}]^T$. That differentiation was necessary because the $Y C_B C_R$ color space is a differential model and for that reason we selected the individual spectral bands that divide the spectrum into almost equal intervals. The next step was converting the images $[R_{641} \ G_{641} \ B_{641}]^T$ and $[R_{532} \ G_{532} \ B_{532}]^T$ to the $Y C_B C_R$ space using Eqn (10) and Eqn (11), where Y denotes the luminance, C_B and C_R are two chromatics channels, which correspond to the color difference model [20]

$$C_B = \frac{0.5}{0.886}(B - Y) \quad (10)$$

$$C_B = \frac{0.5}{0.701}(R - Y) \quad (11)$$

Moreover, since the $YC_B C_R$ transformation is linear, its computational complexity is far lower than that of the $\alpha\beta$ conversion and avoids the logarithm and exponential operations. Like the Reinhard's scheme [22], the resulting quality of the $YC_B C_R$ color transfer method also depends on the images' similarity in composition. The $YC_B C_R$ transformation can be extended into a form Eqn (12) and Eqn (13) [11].

$$\begin{bmatrix} Y_{641} \\ C_{B641} \\ C_{R641} \end{bmatrix} = \begin{bmatrix} 0.2990 & 0.5870 & 0.1140 \\ -0.1687 & -0.3313 & 0.5000 \\ 0.5000 & -0.4187 & -0.0813 \end{bmatrix} \begin{bmatrix} R_{641} \\ G_{641} \\ B_{641} \end{bmatrix} \quad (12)$$

$$\begin{bmatrix} Y_{532} \\ C_{532} \\ C_{532} \end{bmatrix} = \begin{bmatrix} 0.2990 & 0.5870 & 0.1140 \\ -0.1687 & -0.3313 & 0.5000 \\ 0.5000 & -0.4187 & -0.0813 \end{bmatrix} \begin{bmatrix} R_{532} \\ G_{532} \\ B_{532} \end{bmatrix} \quad (13)$$

Next we substituted the blue band of the NEX images with the Y component: $[B_{NEX} C_{B641} C_{R641}]^T, [B_{NEX} C_{B532} C_{R532}]^T$ and next converted them back to the RGB space Eqn (14) and Eqn (15). After that we created a six channel pansharpened image $X_{pansharpened} = [B'_1 B'_2 B'_3 B'_4 B'_5 B'_6]^T$ [11].

$$\begin{bmatrix} Y'_{641} \\ C'_{641} \\ C'_{641} \end{bmatrix} = \begin{bmatrix} 1.0000 & 0.0000 & 1.4020 \\ 1.0000 & -0.3441 & -0.7141 \\ 1.0000 & 1.7720 & 0.0000 \end{bmatrix} \begin{bmatrix} R_{641} \\ G_{B641} \\ B_{R641} \end{bmatrix} = \begin{bmatrix} B'_6 \\ B'_4 \\ B'_1 \end{bmatrix} \quad (14)$$

$$\begin{bmatrix} Y'_{532} \\ C'_{532} \\ C'_{532} \end{bmatrix} = \begin{bmatrix} 1.0000 & 0.0000 & 1.4020 \\ 1.0000 & -0.3441 & -0.7141 \\ 1.0000 & 1.7720 & 0.0000 \end{bmatrix} \begin{bmatrix} R_{532} \\ G_{B532} \\ B_{R532} \end{bmatrix} = \begin{bmatrix} B'_5 \\ B'_3 \\ B'_2 \end{bmatrix} \quad (15)$$

As a result we generated the 6-band MCA image shown in the figure below, whose channels are free from chromatic aberration. Thanks to the decorrelation process, the pansharpened MCA image is characterized by more advantageous correlation coefficients than original fused data, thereby increasing the suitability of the data for image segmentation and classification procedures [4], which, in the case of soil monitoring, is extremely important. For comparative analysis the authors selected a false color band combination (R:MCA6, G:MCA4, B:MCA1), which can be useful for soil and wetlands analyses. In this combination, vegetation appears in different shades of red depending on the types and conditions of the vegetation, since it has a high reflectance in the NIR band. Clear water appears dark-bluish (higher green band reflectance), while turbid water appears cyan (higher red reflectance due to sediments) compared to clear water. Bare soils, roads and buildings may appear in various shades of blue, yellow or grey, depending on their composition [13]. The comparison of the pansharpening process results, carried out by all the methods described above are shown in the figures below – Figure 1.

3. Experimental results

In order to confirm the suitability of the proposed data fusion method for monitoring the soil condition, with particular emphasis on the observation of flood areas and flood plains, additional outdoor tests were carried out. As an object of research, the following samples which simulated different types of soils were used: dry and wet gravel and dry and wet soil. Moreover, in order to ensure accurate and repeatable exposure parameters, a white reference standard was used. The images were acquired from a low altitude with a non-metric digital and multispectral camera and a non-metric digital RGB camera. For the images geometric correction was carried out. Then, the author's method of pansharpening was used and in order to distinguish samples with different levels of moisture, a combination of spectral bands in the range 550–850 nm was chosen. In addition, by using the false color band combination there is a wide possibility of soil and vegetation monitoring. As shown in Figure 2, based on an author's pansharpening method it is easy to distinguish vegetation from both wet and dry samples of soil, which in the case of the original multispectral imagery was not always possible. Additionally, thanks to the high resolution of images collected with Sony NEX-5 camera, fine details of the samples are easy to distinguish, which allow us to perform analyses of pollution of different origins.

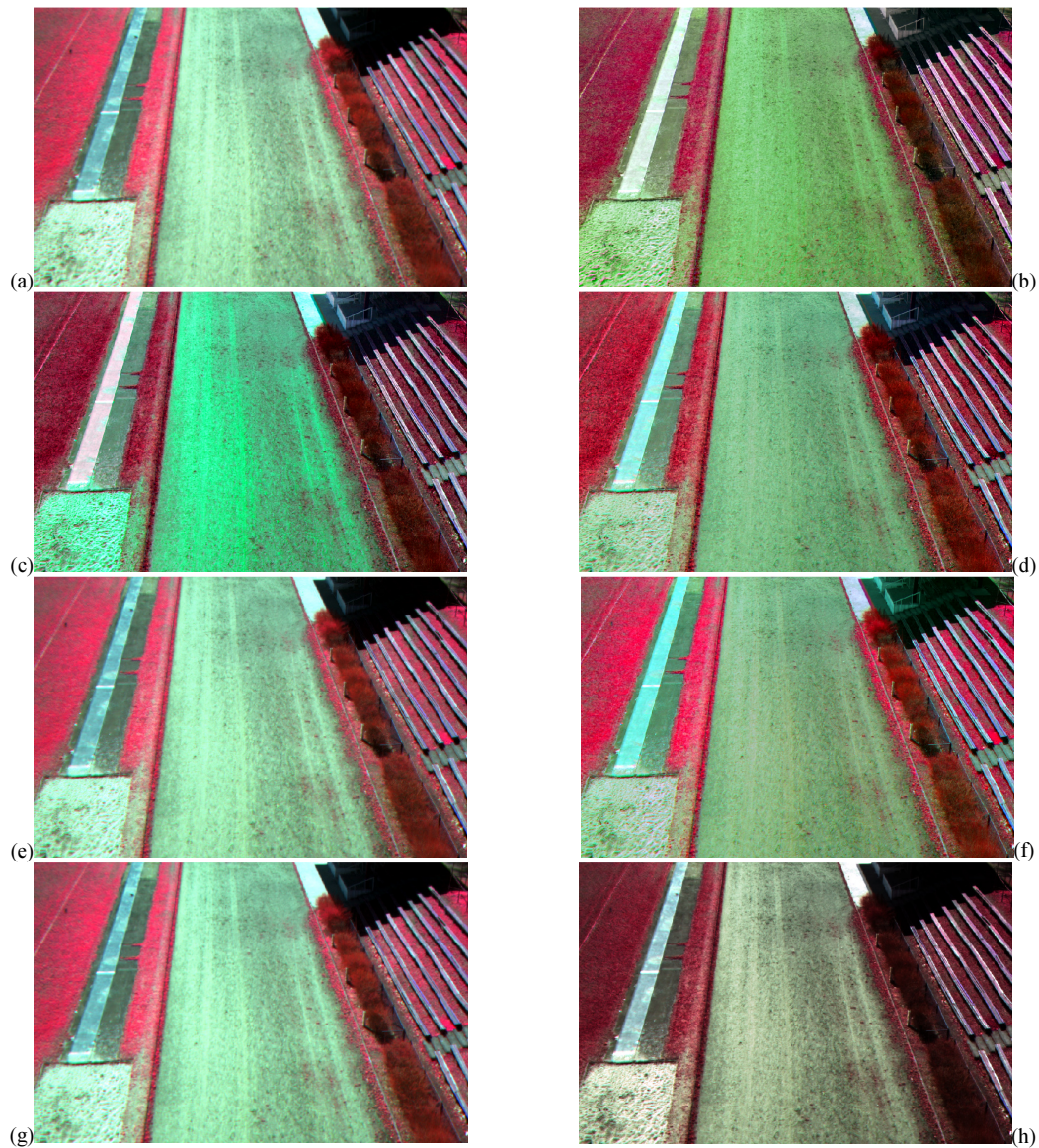


Fig. 1. Original MCA image (a) and after pansharpening using: (b) author's method, (c) Intensity-Hue-Saturation method, (d) Brovey Transformation method, (e) Ehlers Fusion method, (f) Principal Component Analysis method, (g) Wavelet Resolution Merge method, (h) Multiplicative method

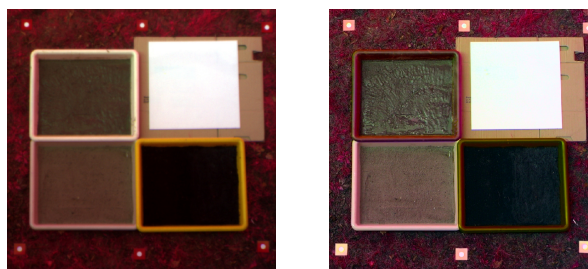


Fig. 2. The results of experiment: original (a) and fused data (b) in the 641 band combination

4. Quality assesment

In literature there are a lot of different approaches to assess the pansharpened images. However, there is not one universal procedure of quality assessment. In addition, the difficulty is the lack of ability of comparing the images after data fusion with reference images which are characterized by both high spatial and spectral resolution [1], [5], [29]. However, there are some methods which at least to some extent overcome this disadvantage. The first method involves the degradation of the spatial resolution of the sharpened image to the resolution of the multispectral image. The second method relies on the degradation of the image with high spatial resolution and multispectral image by the same factor. In both cases, the original image is the reference and is compared with the images after data fusion. These methods can be used to determine parameters based on which it is possible to assess the quality of the fused image. These parameters include a mean error

(RMSE), correlation coefficients, standard deviations and differences in the brightness of the pixels between the images [1, 5, 29]. In order to assess the quality of sharpened images it is reasonable to determine the value of the relative mean error (R-RMSE) instead of RMSE [10]. For the analysis of multispectral images, the following equation Eqn (16) can be used, where DN – the value of the i -th pixel in the k -band.

$$R - RMSE_k = \sqrt{\frac{\sum_{i=1}^N \left(\frac{DN_{fused(k)i} - DN_{original(k)i}}{DN_{original(k)}} \right)^2}{N}} \quad (16)$$

Wald [30] proposed using a global relative error ERGAS Eqn (17), calculated on the basis of RMSE, where h/l is the ratio between the size of the high spatial resolution image pixel and the size of the pixel in the multispectral image with K bands, and $\mu_0(k)$ is the average pixel value of the k^{th} band, for the quality assessment of pansharpened images.

$$ERGAS = 100 \cdot \frac{h}{l} \sqrt{\frac{1}{K} \sum_{k=1}^K \left(\frac{RMSE(k)}{\mu_0} \right)^2} \quad (17)$$

In order to assess the quality of pansharpened images it had been proposed [31] a quality factor Q-Index (also called a quality factor UIQI (Universal Image Quality Index)), which is calculated for each spectral range separately. For the reference image, designated as x , and fused images, marked as y , the Q-Index can be determined from the equation Eqn (18), where σ_{xy} is the covariance between the reference and fused image, $\mu_{0(x)}$, $\mu_{0(y)}$ are the mean values and σ_x^2 , σ_y^2 are variances of the reference and sharpened images.

$$Q = \frac{4\sigma_{xy} \cdot \mu_{0(x)} \cdot \mu_{0(y)}}{(\sigma_x^2 + \sigma_y^2) [(\mu_{0(x)})^2 + (\mu_{0(y)})^2]} \quad (18)$$

Q-Index values are in the range $[-1, 1]$. After converting the formula, the Q-Index can be expressed using three components Eqn (19):

$$Q = \frac{\sigma_{xy}}{\sigma_x \sigma_x} \cdot \frac{2\mu_{0(x)}\mu_{0(y)}}{(\mu_{0(x)})^2 + (\mu_{0(y)})^2} \cdot \frac{\sigma_{xy}}{\sigma_x^2 \sigma_y^2} \quad (19)$$

The first component in the above equation is the correlation coefficient between the multispectral and the sharpened image and has a value range $[-1, 1]$. The second component is sensitive to any bias in the mean of the fused image with respect to the reference image mean. It describes the deviation from the mean value of the original image in comparison to the mean value of sharpened images [5]. This component has a value range $[0,1]$. The third component is a measure of the contrast similarity between the multispectral image and the sharpened image. The ideal value of the index Q is 1 and it could be obtained when the fused image and reference values are equal to each other on a pixel-by pixel basis. In the final discussion of the quality of the sharpened images it should be also known that every method of quality assessment of sharpened images could itself have an effect on the results of quality assessment.

5. Results

When analyzing the values of the three indicators of the spectral data quality, it can be noted that depending on the applied indicator, a different efficiency of each method in the spectral transmission of information is obtained. When analyzing the results of the proposed method of image sharpening for all imagery, it should be noted that the values of indicators will be lower in comparison to traditional methods, which is the result of the assumption that relates to the increasing interpretive values of output imagery (visibility of objects in the shaded area), which result in the large spectral differences between the original and sharpened images. Therefore, in order to make an objective and accurate assessment of the proposed pansharpening method, comparison of quality indicators has been made for a few cases: considering all the processed imagery and their three subsets: the shaded area, areas covered with vegetation and gravel.

It can be seen that the lowest value of the RMSE for the sampled areas was obtained using a wavelet transformation method (Table 1). The results of the proposed method are relatively high, on the all images R-RMSE = 62.96% but after a detailed analysis it can be concluded that the error for the shaded areas is approximately six times greater than R-RMSE of area covered by vegetation and gravel. For this reason, the results of proposed method can be considered as fully satisfactory.

Another indicator of the spectral quality of processed images is ERGAS (Table 2). Wald [30] suggests that if the ERGAS value is less than three, the spectral quality of an image is satisfactory. However, it should be known that the results of the research obtained by Wald [30] are related to the panchromatic and multispectral images recorded from satellite altitudes. In our case, images with different geometries had been processed, obtained at different times from two non-metric digital cameras, which implies a higher value of each indicator. As shown in Table 2, both for the whole image and for each of the parts, the best results were obtained for the wavelet transformation, which, however, has the effect of blurring the image and

reduces interpretation values. The ERGAS index value for the proposed method in relation to all the images is the highest, although its results are similar to the multiplicative transform. However, after a detailed analysis it could be seen that for the shaded area, the ERGAS index is equal to 125.17, while for the vegetation and gravel its value decreases significantly and is about 20, which confirms that for the shaded area, quality statistics are significantly impaired.

Table 1. Relative Root Mean Squared Errors (R-RMSE) between fused MS and original images

R-RMSE								
Area	Bands	IHS	BT	EF	PCA	WT	MT	AUTHORS' METHOD
Entire image	6	25.10%	34.72%	16.33%	7.82%	2.31%	42.15%	109.91%
	4	21.07%	29.28%	9.76%	120.93%	8.36%	42.70%	41.92%
	1	20.79%	30.26%	9.66%	41.11%	5.63%	42.70%	37.06%
	Mean	22.32%	31.42%	11.92%	56.62%	5.43%	42.52%	<u>62.96%</u>
Objects in the shadow	6	27.41%	120.13%	43.79%	19.73%	6.19%	76.21%	434.07%
	4	27.35%	84.98%	19.72%	387.84%	16.76%	76.45%	133.28%
	1	27.34%	71.64%	17.65%	121.42%	10.24%	76.46%	77.62%
	Mean	27.37%	92.25%	27.05%	176.33%	11.06%	76.37%	<u>214.99%</u>
Vegetation	6	20.42%	13.38%	8.27%	7.87%	5.65%	52.85%	24.91%
	4	21.74%	22.21%	11.98%	86.84%	13.14%	52.78%	43.71%
	1	20.74%	28.11%	6.84%	11.68%	4.42%	53.07%	27.71%
	Mean	20.97%	21.23%	9.03%	35.46%	7.73%	52.90%	<u>32.11%</u>
Sand	6	20.30%	9.39%	13.46%	7.25%	7.00%	21.83%	38.10%
	4	6.40%	20.98%	4.92%	11.66%	5.70%	22.57%	31.65%
	1	9.12%	26.86%	5.83%	17.06%	4.72%	22.61%	38.46%
	Mean	11.94%	19.08%	8.07%	11.99%	5.80%	22.34%	<u>36.07%</u>

Table 2. ERGAS values for fused and original images

ERGAS								
Area	Bands	IHS	BT	EF	PCA	WT	MT	AUTHOR'S METHOD
Entire image	6	13.83	9.05	7.09	3.27	0.98	22.84	31.86
	4	7.20	13.47	3.00	17.13	3.05	17.38	18.96
	1	9.01	16.69	3.88	11.35	2.49	18.57	20.28
	Mean	10.01	13.07	4.66	10.58	2.17	19.60	<u>23.70</u>
Objects in the shadow	6	16.41	59.93	23.21	10.62	3.36	43.76	250.54
	4	16.90	36.31	11.16	163.68	8.81	46.15	72.15
	1	16.57	30.43	10.37	51.26	5.46	45.79	52.82
	Mean	16.63	42.22	14.91	75.19	5.88	45.23	<u>125.17</u>
Vegetation	6	11.51	8.03	4.68	4.34	3.23	30.88	13.50
	4	12.97	12.80	6.85	49.13	7.63	30.56	23.92
	1	11.95	16.43	3.95	6.55	2.55	30.66	16.03
	Mean	12.14	12.42	5.16	20.01	4.47	30.70	<u>17.82</u>
Sand	6	11.80	5.69	7.72	4.34	4.20	12.22	21.06
	4	3.57	12.62	3.02	7.29	3.46	12.39	18.53
	1	5.04	16.03	3.47	10.46	2.98	12.33	22.14
	Mean	6.80	11.45	4.74	7.36	3.55	12.31	<u>20.58</u>

Q-Index (Table 3) is another quality indicator which allows the evaluation of the pansharpening results. As in the case of R-RMSE and ERGAS, fusion data using the wavelet transformation gives the most advantageous results, regardless of the test area. In the proposed method Q-Index for the whole image is 0.75, and in comparison with the other data fusion methods it has the best results for the area covered with gravel.

Table 3. Q-Index values for fused and original images. Ideal value 1

Area	Bands	Q-Index						
		IHS	BT	EF	PCA	WT	MT	AUTHOR'S METHOD
Entire image	6	0.76	0.85	0.93	0.99	1.00	0.72	0.63
	4	0.97	0.92	0.99	0.77	0.99	0.93	0.84
	1	0.93	0.84	0.99	0.85	0.99	0.91	0.78
	Mean	0.89	0.87	0.97	0.87	0.99	0.85	0.75
Objects in the shadow	6	0.71	0.52	0.85	0.96	0.99	0.40	0.15
	4	0.87	0.83	0.96	0.39	0.97	0.39	0.63
	1	0.86	0.83	0.96	0.75	0.99	0.38	0.69
	Mean	0.81	0.73	0.92	0.70	0.98	0.39	0.49
Vegetation	6	0.40	0.40	0.83	0.98	1.00	0.46	0.43
	4	0.22	0.68	0.86	0.29	0.85	0.59	0.49
	1	0.10	0.16	0.61	0.31	0.86	0.46	0.24
	Mean	0.24	0.41	0.77	0.53	0.90	0.50	0.39
Sand	6	0.26	0.57	0.46	0.73	0.77	0.80	0.51
	4	0.89	0.57	0.91	0.59	0.88	0.88	0.76
	1	0.83	0.69	0.90	0.71	0.92	0.89	0.72
	Mean	0.66	0.61	0.76	0.68	0.86	0.86	0.66

The values of the above indicators show that the results of the proposed method can be considered as satisfactory, since areas covered by vegetation or gravel are similar, and in many cases better than, the results of classical pansharpening methods. The relatively high values of indicators for shaded areas do not eliminate this method from further consideration, and even confirm its effectiveness and usability for research concerning monitoring of flooded areas. This is justified by the fact that the acquisition of imagery from a low ceiling and for different lighting conditions often results in relatively more shading of the scene, for example, by trees and buildings. Using the proposed method of pansharpening allows full use of the information acquired with a multispectral camera, which will expand opportunities of an objects detection and improve the interpretative values of the output image. Although the most favorable values of indicators were achieved for the pansharpened image created using wavelet transformation, it can not be regarded as being the best result. This is due to the fact that this method uses a filtration process and as a result, the high resolution of image is not fully utilized and thus the quality of the resulting images and their usefulness in a lot of analyses is significantly decreased.

6. Conclusion

This paper presents the results of research on data fusion of high resolution images and multispectral images acquired from a variety optoelectronic sensors. As a result of research the method of data integration based on an independent geometric correction of each spectral band of multispectral images, transformation to $YC_B C_R$ color space and converting the luminance component to the blue band of high resolution image acquired with non-metric cameras was proposed. Aa analysis of the traditional pansharpening methods for images acquired from different sensors was done and a qualitative analysis of the output imagery using spectral quality assessment indicators: R-RMSE, EGRAS and the ratio of Q-Index was conducted. The output image of the proposed method is characterized by much higher interpretation values than the other presented image fusion methods. Thanks to the decorrelation of multispectral data is an ideal base to carry out a lot of research, even in the shaded areas. In conclusion, the proposed method of data integration of images acquired for example from an unmanned aerial vehicle could find applications in remote sensing research of soil, water, flooded areas and floodplains which had been confirmed by the results of research that was conducted in an environment similar to the natural (outdoor).

References

- [1] Aiazzi, B.; L. Alparone,; S. Baronti, 2002. Context driven fusion of high spatial and spectral resolution images based on oversampled multiresolution analysis, *IEEE Transactions on Geoscience and Remote Sensing* 40(10): 2300–2312. <http://dx.doi.org/10.1109/TGRS.2002.803623>
- [2] Alley, R. 1999. Algorithm Theoretical Basis Document for: Decorrelation Stretch, *Jet Propulsion Laboratory*, Pasadena, 5–7 p.
- [3] Arnold, T.; De Biasio, M.; Fritz, A.; Leitner, R. 2010. UAV-based multispectral environmental monitoring, *Sensors*, 2010 *IEEE*, 995–998.
- [4] Benedetti, R.; Rossini, P.; Taddei, R. 1994. Vegetation classification in the middle Mediterranean area by satellite data, *REMOTE SENSING* 15(3): 583–596. <http://dx.doi.org/10.1080/01431169408954098>
- [5] Cakir, H. I.; Khorram, S. 2008. Pixel level fusion of panchromatic and multispectral images based on correspondence analysis, *Photogrammetric Engineering and Remote Sensing* 74(2): 183–192. <http://dx.doi.org/10.14358/PERS.74.2.183>
- [6] Chavez, P. S.; Sides, S.; Anderson, J. 1991. Comparison of three different methods to merge multiresolution and multispectral data: Landsat TM and SPOT panchromatic, *Photogrammetric Engineering & Remote Sensing* 57(3): 295–303.
- [7] Dabrowski, R.; Orych, A.; Walczykowski, P. 2013. Evaluation of the possibility of using the miniMCA multispectral camera in Imagery Intelligence RCITD, in *International Virtual Research Conference In Technical Disciplines*, Slovakia ISBN-978-80-554-08-07-1, ISSN 1339-5076. <http://dx.doi.org/10.1117/12.514078>
- [7] Ehlers, M. 2004. Spectral Characteristics Preserving Image Fusion Based on Fourier Domain Filtering, in *Remote Sensing for Environmental Monitoring, GIS Applications, and Geology IV*, Proceedings of SPIE, Ehlers, M., H.J. Kaufmann and U. Michel (Eds.) Bellingham, WA, 1–13.
- [8] González-Audiciana, M.; Otazu, X. 2004. Comparison between Mallat's and the a'trous discrete wavelet transform based algorithms for the fusion of multispectral and panchromatic images, *International Journal of Remote Sensing* 26(3): 595–614. <http://dx.doi.org/10.1080/01431160512331314056>
- [9] Helmy, A. K.; Nasr, A. H.; El-Taweel, Gh. S. 2010. Assessment and Evaluation of Different DataFusion Techniques, *International Journal of Computers* 4(4): 107–115.
- [10] Kroll, C.; Stedinger, J. 1996. Estimation of moments and quantiles using censored data, *Water Resources Research* 32(4): 1005–1012. <http://dx.doi.org/10.1029/95WR03294>
- [11] Li, G. 2011. *Image Fusion Based on Color Transfer Technique*, Image Fusion and Its Applications Edited by Dr. Yufeng Zheng, 55–71.
- [12] Li, H.; Manjunathe, B. S.; Mitra, S. K. 1995. Multisensor image fusion using the wavlet transform, *Graphical Models and Image Processing* 27(3): 235–244. <http://dx.doi.org/10.1006/gmip.1995.1022>
- [13] Liew, S. C. 2001. Interpreting optical remote sensing images URL: http://www.crisp.nus.edu.sg/~research/tutorial/opt_int.htm (last date accessed: 20 May 2013).
- [14] Lucieer, A.; Robinson, S.; Turner, D.; Harwin, S.; Kelcey, J. 2012. Using a micro-UAV for ultra-high resolution multi-sensor observations of antarctic moss beds. *ISPRS - International Archives of the Photogrammetry, Remote Sensing and Spatial Information Sciences* Vol. XXXIX-B1: 429–433.
- [15] Meenakshisundaram, V. 2005. *Quality assessment of IKONOS and QuickBird fused images for urban mapping*, M.S. thesis, Univ. Calgary, Calgary, AB, Canada, 1–118 .
- [16] Nikolakopoulos, K. G. 2008. Comparison of nine fusion techniques for very high resolution data, *Photogrammetric Engineering and Remote Sensing* 74(5): 647. <http://dx.doi.org/10.14358/PERS.74.5.647>
- [17] Parcharidis, I.; Kazi-Tani, L. M. 2000. Landsat TM and ERS data fusion: a statistical approach evaluation for four different methods, *Proceedings of the international geoscience and remote sensing symposium, IGARSS 2000* 5: 2120–2122.
- [18] Pohl C. and Van Genderen J. L. 1998. Multisensor image fusion in remote sensing: Concepts, methods, and applications, *International Journal Remote Sensing*, 19 (5): 823–854. <http://dx.doi.org/10.1080/014311698215748>
- [19] Pradhan, P. S.; King, R. L.; Younan, N. H.; Holcomb, D. W. 2006. Estimation of the number of decomposition levels for a waveletbased multiresolution multisensor image fusion, *IEEE Transactions on Geoscience and Remote Sensing* 44(12): 3674–3683. <http://dx.doi.org/10.1109/TGRS.2006.881758>
- [20] Poynton, C. 2003. *Digital Video and HDTV, Algorithms and Interfaces*, Morgan Kaufmann, San Francisco, CA, 430 p.
- [21] Ranchin, T.; Wald, L. 2000. Fusion of high spatial and spectral resolution images: the ARSIS concept and its implementation, *Photogrammetric Engineering & Remote Sensing* 66(1): 49–61.
- [22] Reinhard, E.; Ashikhmin, M.; Gooch, B.; et al. 2001. Color Transfer between Images, *IEEE Comput. Graph. Appl.* 21(5): 34–41. <http://dx.doi.org/10.1109/38.946629>
- [23] Schowengerdt, R. A. 1980. Reconstruction of multi-spatial, multi-spectral image data using spatial frequency content, *Photogrammetric Engineering & Remote Sensing* 46(10): 1325–1334.
- [24] Shah, V. P.; Younan, N. H.; King, R. L. 2008. Efficient Pan-Sharpening Method via a Combined Adaptive PCA Approach and Contourlets, *IEEE Transactions on Geoscience and Remote Sensing* 46(5): 1323–1335. <http://dx.doi.org/10.1109/TGRS.2008.916211>
- [25] Sohn, S. Y.; Lee, S. H. 2002. Data fusion, ensemble and clustering to improve the classification accuracy for the severity of road traffic accidents in Korea, *Safety Science* 41(2003): 1–14. [http://dx.doi.org/10.1016/S0925-7535\(01\)00032-7](http://dx.doi.org/10.1016/S0925-7535(01)00032-7)
- [26] Strang, G. 1988. *Linear Algebra and its Applications*. San Diego: Harcourt Brace Jonanovich, 3rd ed., p. 36.
- [27] Vijayaraj, V.; O'Hara, C. G.; Younan, N. H. 2004. Quality analysis of pansharpened images. In *Geoscience and Remote Sensing Symposium, 2004. IGARSS'04. Proceedings. 2004 IEEE International* (1): 85–88.
- [28] Vrabel, J. 1996. Multispectral Imagery Band Sharpening Study, *Photogrammetric Engineering & Remote Sensing* 62(9): 1075–1083.
- [29] Wald, L.; Ranchin, T.; Mangolini, M. 1997. Fusion of satellite images of different resolutions: Assessing the quality of resulting images, *Photogrammetric Engineering & Remote Sensing* 63(6): 691–699.
- [30] Wald, L. 2002. *Data Fusion: Definitions and Architectures – Fusion of Images of Different Spatial Resolutions*, Les Presses, Ecole des Mines de Paris, Paris, France, 200 p.
- [31] Wang, Z.; Bovik, A.C. 2002. A universal image quality index, *IEEE Signal Processing Letters* 9(3): 81–84. <http://dx.doi.org/10.1109/97.995823>
- [32] Zhou, J.; Civco, D. L.; Silander, J. A. 1998. A wavelet transform method to merge Landsat TM and SPOT panchromatic data, *International Journal of Remote Sensing* 19(4): 743–757. <http://dx.doi.org/10.1080/014311698215973>